Publication Year	2017
Acceptance in OA	2020-08-28T12:29:43Z
Title	The Calern Asteroid Polarimetric Survey using the Torino polarimeter: assessment of instrument performances and first scientific results
Authors	Devogèle, M., CELLINO, Alberto, Bagnulo, S., Rivet, J. P., Bendjoya, P., Abe, L., PERNECHELE, Claudio, Massone, G., Vernet, D., Tanga, P., Dimur, C.
Publisher's version (DOI)	10.1093/mnras/stw2952
Handle	http://hdl.handle.net/20.500.12386/26949
Journal	MONTHLY NOTICES OF THE ROYAL ASTRONOMICAL SOCIETY
Volume	465

MONTHLY NOTICES of the Royal Astronomical Society

The Calern Asteroid Polarimetric Survey using the Torino Polarimeter: assessment of instrument performances and first scientific results

Journal:	*Monthly Notices of the Royal Astronomical Society*
Manuscript ID	MN-16-0958-MJ.R1
Manuscript type:	Main Journal
Date Submitted by the Author:	30-Aug-2016
Complete List of Authors:	Devogèle, Maxime; Université de Liège, Space sciences, Technologies and Astrophysics Research; Observatoire de la Cote d\'Azur Nice, Lagrange Cellino, Alberto; INAF, Osservatorio Astrofisico di Torino Bagnulo, Stefano; Armagh Observatory, Rivet, Jean-Pierre; Universite de Nice Sophia-Antipolis, Laboratoire Lagrange UMR 7293 Bendjoya, Philippe; UMR 6525 H. Fizeau, Université de Nice Sophia Antipolis/ CNRS/ Observatoire de la Côte d'Azur, Abe, Lyu; CNRS-OCA, Lagrange Pernechele, Claudio; INAF - Osservatorio Astronomico di Padova Massone, Giuseppe; INAF, Osservatorio Astrofisico di Torino Vernet, David; Observatoire de la Cote d\'Azur Nice, Lagrange Tanga, Paolo; Observatoire de la Cote d'Azur, Laboratoire Cassiopee DIMUR, Cecile; Universite de Nice Sophia-Antipolis, Laboratoire Lagrange UMR 7293
Keywords:	minor planets, asteroids, general < Planetary Systems, surveys < Astronomical Data bases, polarization < Physical Data and Processes

SCHOLARONE™
Manuscripts

Mon. Not. R. Astron. Soc. **000**, 1–?? (2002) Printed 30 August 2016 (MN LATEX style file v2.2)

The Calern Asteroid Polarimetric Survey using the Torino Polarimeter: assessment of instrument performances and first scientific results

M. Devogèle[1,2], A. Cellino[3], S. Bagnulo[4], J.P. Rivet [2], P. Bendjoya[2], L. Abe[2], C. Pernechele[5], G. Massone[6], D. Vernet[2], P. Tanga[2], and C. Dimur[2],
[1] *Université de Liège, Space sciences, Technologies and Astrophysics Research (STAR) Institute, Allée du 6 Août 19c, Sart Tilman, 4000 Liège, Belgium*
[2] *Laboratoire Lagrange, UMR7293, Univ. Côte d'Azur, CNRS, Obs. de la Côte d'Azur, Bv de l'Observatoire, S 34229, 06304 Nice, France*
[3] *INAF - Osservatorio Astrofisico di Torino, Pino Torinese, Italy*
[4] *Armagh Observatory, College Hill, Armagh BT61 9DG, UK*
[5] *INAF - Osservatorio Astronomico di Padova, Padova, Italy*
[6] *INAF - Osservatorio Astrofisico di Torino, Pino Torinese, Italy*

ABSTRACT

A new polarimeter based on the Wedged double Wollaston concept has been built at the Torino Observatory and installed on a 1-meter telescope at the Calern observing station of the "Observatoire de la Côte d'Azur (France)". Its main purpose is to carry out a polarimetric survey of minor Solar System objects, named CAPS (Calern Asteroid Polarimetric Survey). In this paper, the new Torino Polarimeter (ToPol) and the results of preliminary scientific validation tests are described. A number of standard stars with known polarization states, as well as a number of asteroids for which the polarimetric properties are known, have been observed in order to assess the instrument accuracy. The instrumental polarization has been found to be stable within a few 10^{-4} units. A total of 124 new polarimetric observation of 78 asteroids are presented. In the case of asteroids already observed in the past, the new data are in agreement with available phase-polarization curves with error bars smaller than most previously published data. We present also data for 21 asteroids than were never observed before in polarimetry.

Key words: asteroids – polarization – instruments: polarimeter

1 INTRODUCTION

Polarimetry is an important tool to obtain a physical characterization of small Solar System bodies. The change of linear polarization of scattered sunlight in different illumination conditions can provide information about some properties of the layer of regolith covering the surfaces of atmosphereless Solar System bodies (Petrova et al. 2004). In particular, polarimetry is a primary technique to determine the geometric albedo of the surfaces (Cellino et al. 2015b). Recent review papers of this subject have been published by Cellino et al. (2015a) and Belskaya et al. (2015), where interested readers will also find updated lists of bibliographic references. An analysis of the dependence of linear polarization upon wavelength has been published by Bagnulo et al. (2015).

The primary goal of classical asteroid polarimetry is to determine the so-called *phase - polarization curve*. This curve describes the change of the fraction of linear polarization as a function of phase angle (*i.e* the angle between the directions to the Sun and to the observer, as seen from the target body). For reason of symmetry, the plane of linear polarization of asteroids is almost always either coincident with or perpendicular to the scattering plane (*i.e.* the plane containing the Sun, the object and the observer) (see, for instance, Dollfus et al. 1989; Zellner & Gradie 1976). As a consequence, the state of linear polarization of asteroids is usually expressed in terms of the flux difference between the scattered sunlight components having polarization plane perpendicular and parallel to the scattering plane, normalized to their sum :

$$P_{\rm r} = \frac{I_\perp - I_\parallel}{I_\perp + I_\parallel}. \quad (1)$$

© 2002 RAS

P_r can be either positive or negative according to the direction of the plane of linear polarization with respect to the scattering plane. However, its module is almost always equal to the degree of linear polarization. The range of phase angle for which P_r is negative is commonly called the *negative polarization branch*. P_r has the advantages to convey simultaneously information of the fraction of linear polarization and the orientation of the plane of polarization for solar system objects.

In the past, the progress in the field of asteroid polarimetry has been slowed down due to a general lack of dedicated instruments. In this paper, we describe the first results of a dedicated survey making use of a new polarimeter built at the Astrophysical Observatory of Torino (Italy). This work extends and improves some preliminary results presented in Devogèle et al. (2015).

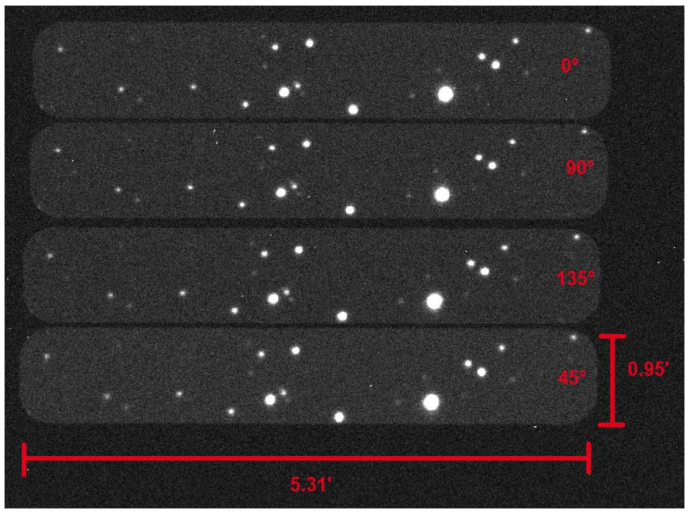

Figure 1. Example of a ToPol frame. The four strips correspond to the four images of the field of view of ToPol. Each strip corresponds to one specific polarization state (respectively from top to bottom 0°, 90°, 135° and 45°).

2 INSTRUMENT DESCRIPTION

The determination of the degree of linear polarization requires the measurement of the intensities of light components produced by the splitting of an incident light beam. An accurate measurement of linear polarization requires therefore high signal-to-noise (S/N) photometric measurements, especially in cases, like asteroid polarimetry, in which the fraction of linear polarization is intrinsically quite low (in most cases, below 1%).

The splitting of the incoming light beam in linear polarization measurements is produced by optical devices like Wollaston prisms. The polarimeter described in this paper is based on a Wedged double Wollaston configuration (Oliva 1997). It has been designed by one of us (CP) and is described by Pernechele et al. (2012). This instrument is very similar to another one designed by the same author, that in the past was operational at the Asiago Observatory (Italy) (Fornasier et al. 2006), and is currently operational at the NOT (Nordic Optical Telescope) telescope at La Palma, Canary islands (Spain) (Fornasier et al. 2015). Our new ToPol (for Torino Polarimeter) instrument is installed at the Cassegrain focus (F/12.5) of the 1.04m "Omicron" (West) telescope of the C2PU (*Centre Pédagogique Planète et Univers*) facility, located on the Calern plateau and managed by the Observatoire de la Côte d'Azur, France (IAU code: 010). The field of view is 5.31×0.95 arcmin^2 for the ToPol instrument.

The new polarimeter is mainly devoted to carry out a dedicated program of asteroid observations, the "Calern Asteroid Polarimetric Survey" (CAPS).

Thanks to the use of a Wedged double Wollaston as analyser, both Q/I and U/I can be measured simultaneously with only one exposure. The Wedged double Wollaston prism splits the incoming light beam into four separate components, corresponding to the 0°, 90°, 45° and 135° linear polarization states. It produces four simultaneous images on the focal plane, which are seen as clearly separated stripes on the CCD detector. An example of a ToPol frame is displayed in Fig. 1.

A scheme and a photography of the ToPol instrument is displayed in Fig. 2.

By measuring the photometric fluxes of the four polarized images one gets all the polarimetric information needed to compute P_r, after some calibration steps (see Section 3).

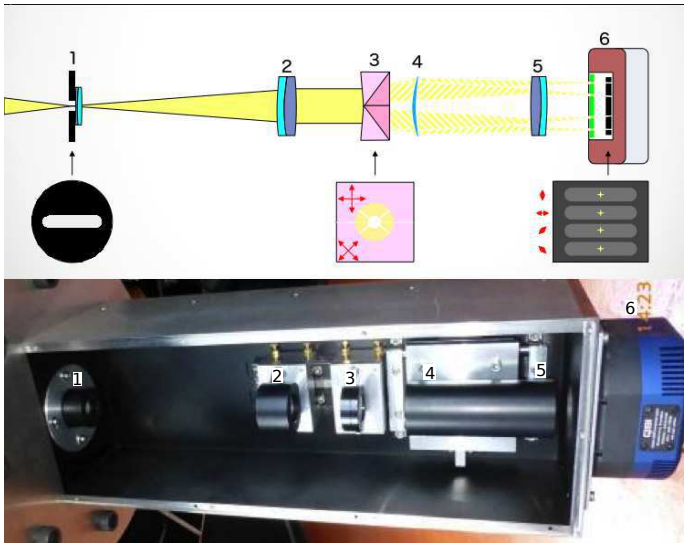

Figure 2. Scheme and photography of the ToPo instrument. 1: Field stop followed by the field lens. 2: Collimator lens. 3: Wedged double Wollaston. 4 and 5: Camera optics. 6: QSI632 CCD camera

The CCD camera attached to the ToPol instrument is a QSI632ws. It is equipped with a KAF-3200ME sensor of 2184×1472 pixels and a filter wheel with classical Johnson-Cousins UBVRI filters. Analyses of flat fields shows that the CCD has currently no dead pixels. Dark frame analyses shows that only 24 isolated pixels possess high dark current value.

3 DATA REDUCTION PRINCIPLES FOR POLARIMETRY

To measure the fraction of linear polarization of our targets, standard CCD-reduction techniques are first applied (dark frame subtraction and flat-field correction). Then, aperture photometry is applied to all four separate sub-images of the target. A growth curve strategy is applied to optimize the aperture sizes (see below). This yields the values of the four polarized components I_0, I_{45}, I_{90}, and I_{135}. The reduced Stokes parameters q and u are then computed according to their standard definitions (Shurcliff 1962) :

$$q = \frac{Q}{I} = \frac{I_0 - I_{90}}{I_0 + I_{90}}, \tag{2}$$

$$u = \frac{U}{I} = \frac{I_{45} - I_{135}}{I_{45} + I_{135}}, \tag{3}$$

where I, Q and U are the standard Stokes parameters. Finally, the total polarization degree P and the position angle θ of the linear polarization plane with respect to the instrument's zero direction are obtained from :

$$P = \sqrt{q^2 + u^2}, \tag{4}$$

$$\theta = \frac{1}{2} \arctan \frac{u}{q}. \tag{5}$$

Note that the relation between P and the P_r parameter defined in Sec. 1, which is usually adopted in polarimetric studies of small solar system bodies, is simply :

$$P_r = P \cdot \cos(2\phi)$$

where ϕ is the angle between θ and the position angle of the plane perpendicular to the scattering plane (Zellner & Gradie 1976).

The reduced Stokes parameters q and u are related to the instrument's internal reference plane, which is not necessarily aligned exactly along the standard reference direction for astronomical polarimetry *i.e.* the celestial North direction according to IAU recommendations. Moreover, these parameters are likely to be biased by the instrumental response. Thus, a careful instrumental calibration is required (see Sec. 4).

3.1 Curve of growth

The fraction of linear polarization for main belt asteroids is relatively small (usually of the order of 1% or less, the highest values of P_r rarely exceeding $\pm 2\%$). So, high photometric accuracy in the measurement of the four images of the target is required. PSF fitting or optimal image subtraction techniques cannot be applied, since the field of view of the instrument is narrow and in general no suitable reference stars may be found in the field of view. Thus, aperture photometry is used to extract the four polarized fluxes. The measured values of the Stokes parameters are sensitive to the size of the photometric aperture. In order to obtain more accurate results, we adopt the "Curve of growth" approach suggested by Bagnulo et al. (2011, 2015). This technique consists of measuring the values q and u given by Eqs. 2 and 3 as a function of the aperture. Usually, the q and u values converge to an asymptotic value much faster than the values of the flux on the individual apertures. The choice of the best aperture is a compromise between reaching a plateau and keeping the lowest possible error bar (which at larger aperture may be dominated by background noise, hence increases with the aperture size). An example of such a curve of growth is given in Fig. 3.

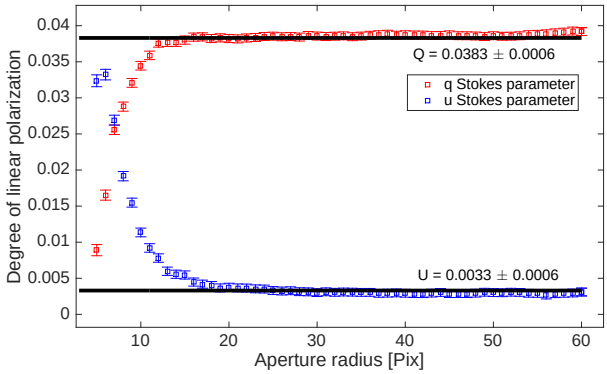

Figure 3. Example of a typical curve of growth. The red squares represent the q reduced Stokes parameter as a function of the aperture radius (in pixels). The blue ones correspond to the u reduced Stokes parameters. The black lines represent the best value of q and u. The u curve was reversed for display reasons.

A first estimation of the sky background is made by taking the average value of the pixels in an annulus around the target. The second step consist in building a curve of growth of the flux of the target (with sky background subtracted). For great aperture radii, the curve of growth should become flat, since external pixels only contain background flux (in the assumption that the background is linear with pixel location). If this is not the case, the sky background is adjusted until the growth curve shows a flat trend. The correction to the sky background is kept small and smaller than three times the standard deviation of the sky background pixel values.

4 ASSESSMENT OF INSTRUMENTAL POLARIZATION AND ITS STABILITY

Imperfection of the optical and mechanical properties of ToPol, as of any other polarimeter, produce spurious polarization of the incoming light. These spurious polarization, called instrumental polarization, is due to asymmetry on the optics, non normal reflection effects, as well as artificial polarization effects due to different transmission coefficients along the light path of the four images of the source.

Due to the effect of instrumental polarization, the results of polarimetric measurements are not simply the normalized Stokes parameters q and u, but rather a couple of parameters q' and u' defined as:

$$q' \simeq q + q_0, \tag{6}$$

$$u' \simeq u + u_0, \tag{7}$$

where q_0 and u_0 are due to instrumental polarization effects.

Both q_0 and u_0 can be determined by means of measurements of standard unpolarized stars (for which the q and u parameters are supposed to be identically null), and can then be subtracted to subsequent observations. In addition, the measurement of highly-polarized, standard stars allows to

correct for the offset between the on-sky North direction and the zero instrumental direction. (for a list of standard stars for linear polarization, see, e.g., Hsu and Breger (1982); Turnshek et al. (1990); Gehrels (1974)).

The stability over time of the instrumental polarization must be assessed by repeating standard stars measurements. In particular, the adopted observing procedures require that during each observing night at least two zero-polarization and one high-polarization standard stars are measured (see App. A for extended tables of ToPol observation of standard stars).

However, the most important feature to be checked is not simply the absolute value of the instrumental bias affecting the determination of the q and u parameters, but rather the stability of this instrumental bias. The stability must be assessed over both short term (one single night) as well as over long term (several nights in the same session, or even several sessions). Short term stability of instrumental offsets is the minimal requirement for the calibration process to be reliable and accurate.

The stability of the instrumental polarization was determined by measuring 500 times the same standard polarized stars during an entire 8 hours night (HD90508, $m_V = 6.5$, see Gehrels (1974)). The standard deviation of these 500 measurements was found to be 1.1×10^{-4} for q and 1.8×10^{-4} for u. Thus, the instrumental stability on the short term (one night) does not appear to be a limiting factor for ToPol.

In February and March 2015, 8 full nights were devoted to measurements of instrumental polarization. Seventeen unpolarized standard stars were observed. The observing circumstances of all the observations are given in the App. A. From these measurements we could determine with a good accuracy the amount of instrumental polarization and its stability over a period of time of about one month. From these data, the instrumental polarization coefficients were found to be :

$$q_0^{(V)} = 3.834 \times 10^{-2} \pm 1.0 \times 10^{-4}, \quad (8)$$

$$u_0^{(V)} = 3.04 \times 10^{-3} \pm 1.7 \times 10^{-4}, \quad (9)$$

in the V band, and :

$$q_0^{(R)} = 3.641 \times 10^{-2} \pm 1.0 \times 10^{-4}, \quad (10)$$

$$u_0^{(R)} = 2.90 \times 10^{-3} \pm 1.9 \times 10^{-4}, \quad (11)$$

in the R band.

The measurements of 9 highly-polarized standard stars during the first year of observation showed that ToPol is rotated by $0.7° \pm 0.4°$ with respect to the IAU convention for the zero direction of polarization. The residuals between the known polarization for these standard stars and the polarization measured by ToPol after removal of the instrumental bias and rotation is 2×10^{-4}. However, these results have to be taken with caution. Indeed, it was reported by Hsu and Breger (1982); Bastien et al. (1988, 2007) that most of the stars which are qualified as high-polarized standard may show variability in polarization.

5 EXPECTED SIGNAL-TO-NOISE RATIO

The expected errors on q and u can be computed using the following relation (Bagnulo et al. 2006):

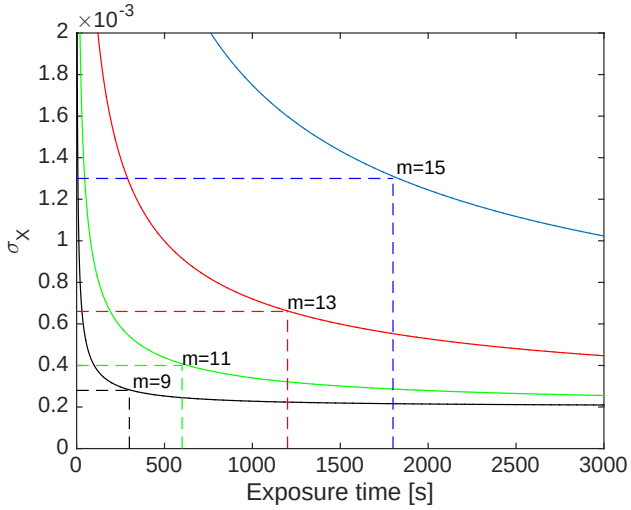

Figure 4. Expected error bar in function of exposure time for different targets magnitude. The dashed lines correspond to the typical cumulative exposure time used for different source magnitude.

$$\sigma_X = \frac{1}{\sqrt{F}}, \quad (12)$$

where σ_X corresponds to the expected errors on the q or u parameter and F is the total flux from the two beams used to compute q or u. Based on the Eq. (12), the expected error bars for observations of targets having different apparent magnitudes as a function of exposure time can be computed using an equation of the type

$$\sigma_X = \frac{1}{\sqrt{t_{\rm exp} 10^{-0.4(m-a)}}}, \quad (13)$$

where $t_{\rm exp}$ is the exposure time, m the magnitude of the target and a a parameter corresponding to the zero instrumental magnitude.

The a parameter for the ToPol instrument attached to the Omicron 1.04 meter telescope (ToPol@C2PU) was empirically determined from the observation of targets of different magnitude. A systematic error should be added to the result of Eq. (13) to take into account the error made on the estimation of the instrumental polarization. This error is estimated to 2×10^{-4}. Figure 4 represent the expected error bars as function of exposure time and magnitude of the target.

Setting the limiting magnitude to 15, ToPol@C2PU can measure the full phase-polarization curve for more than 650 different asteroids. For a 15 magnitude asteroid, a 30 minutes cumulative exposure time will result in an accuracy of 1.3×10^{-3}. In the case of a limiting magnitude of 13, the full phase-polarization of more than 160 asteroids can still be measured. The expected error bar on a 13 magnitude asteroid is 6.5×10^{-4} with a cumulative exposure time of 20 minutes. Finally, if we restrict to asteroids brighter than the 11th magnitude, only a little bit more than 20 asteroids can be fully covered. However, the accuracy can be as good as 0.4×10^{-4} with only 10 minutes exposure time. For brighter objects, the instrumental polarization become the dominant source of errors.

6 FIRST RESULTS OF THE CALERN ASTEROID POLARIMETRIC SURVEY

In this section, we present a preliminary data base of asteroid polarimetric measurements including 124 entries, referring to a total of 78 asteroids observed in the first operational phase of CAPS. Most data consist of single measurements of objects in the standard Johnson V filter, but several objects have also a measurement in standard R colour, while in five cases only an R measurement is available. The whole data base is given in the App. B. For each measurement we list the number of the asteroids, the observation date, the corresponding phase angle, the $P_{\rm r}$ and its associated uncertainty (both in % unit), and the adopted filter, respectively. Generally, we have obtained so far only one or two different polarization measurements per object. Our data base includes a large variety of asteroids belonging to different taxonomic classes. The linear polarization of some objects has never, or very rarely been measured before. Some objects have a reliable estimate of the geometric albedo, and they can be used to calibrate the existing relations between albedo and polarimetric behaviour (see Cellino et al. (2015b) for further details). Some objects may also belong to dynamical families. Our reference for this, among differently published family lists, is Milani et al. (2014).

In what follows, we limit our analysis to polarimetric measurements obtained in V. When browsing published V polarimetric data available in the literature, in order to compare them with our CAPS data, we selected only measurements having uncertainties not larger than 0.2%, since CAPS data are generally of a much better quality. As for literature data, we used the polarimetric data bases available at the PDS web site[1]. Moreover, we also used some polarimetric measurements obtained at the CASLEO observatory (Argentina), and published by Gil Hutton et al. (2014).

Asteroid phase-polarization curves have generally a common morphology, characterized by a negative polarization branch followed, after an "inversion angle" $\alpha_{\rm inv}$ (generally at a phase angle around 20°) by a linear increase of $P_{\rm r}$. They can be suitably represented by the following relation (Muinonen et al. 2009):

$$P_{\rm r}(\alpha) = A \cdot [e^{(-\alpha/B)} - 1] + C \cdot \alpha \qquad (14)$$

where α is the phase angle, and A, B, C are parameters to be derived by least-squares techniques (see Cellino et al. (2015b) and Cellino et al. (2016)). We used the above relation to compute best-fits of available data for objects for which a sufficient number of measurements is available, as shown in some of the Figures presented below.

CAPS data can be classified in different categories. There are previously well-observed (and generally bright) asteroids, for which we want to check that CAPS data are in agreement with already existing phase-polarization curves. Examples: asteroids (2), (3), (6), (7), (8), (10), (18), (20), (42), (44), (51), (192), (234), (324), (511).

For these asteroids, the new CAPS data are in agreement with previously derived phase - polarization curves in all the cases(14 asteroids observed in V light), with the only exception of one single CAPS measurement of asteroid (192) Nausikaa, which is found to show a lower value of positive polarization at a phase angle of about 33°, with respect to previously available measurements. Moreover, the nominal error bars of CAPS data tend also to be comparable with, if not better than, most data available in the literature. Four cases, including the discrepant case of Nausikaa, which certainly deserves further observations, are shown in Fig. 5. The other three asteroids shown in this Figure 5 are (2) Pallas, (44) Nysa, and (511) Davida, which belong to the taxonomical classes B, E and C, respectively, according to the old classification of Tholen (1984)[2].

Our data base includes a large variety of asteroids belonging to different taxonomic classes. As it is well known, two major taxonomic complex, S and C, dominate the asteroid main belt population, and can also be split into a number of separate sub-classes (see, for instance, Bus & Binzel (2002)). S-class asteroids have moderate albedo and orbit mostly in the inner region of the belt, so it is not unexpected that they account for a large fraction of the objects observed so far by the CAPS. In particular, if we consider only asteroids for which measurements in standard V are available, 25 of them (out of 74) belong unambiguously to the S-complex. Our polarimetric measurements for asteroids (26), (57), (61), and (103) are the first data obtained for these objects, and share the known polarimetric behaviour already known for objects of this class, as shown, as an example, in Fig. 6 in the case of the asteroid (26) Proserpina.

Some other S-class asteroids had several polarimetric measurements already available in the literature, and the new CAPS data are consistent with them. In some cases, including for instance asteroids (17), (23) and (478), the new data improve the phase coverage allowing us to derive best-fit curves according to Eq. (14).

We also obtained one single measurement for the asteroid (71) Niobe, whose taxonomic classification is uncertain, the old S-class proposed by Tholen (1984) having been more recently not confirmed by Bus & Binzel (2002), who propose rather an Xe classification (see also (Fornasier et al. 2006)). In this context, the CAPS measurement obtained at a phase angle of 7.6 deg is not decisive, being marginally compatible with both classifications, although the Bus & Binzel (2002) interpretation looks more plausible.

Asteroids belonging to the C class have low albedo and dominate the asteroid inventory in the outer regions of the main belt. In general terms, C-class asteroids tend therefore to be fainter than S objects of the same size. Nevertheless, these objects are as abundant as S-class asteroids in the CAPS database (in V colour), including 24 objects out of 74.

[1] *Planetary Data System*. The data are available at the URL address http://pds.jpl.nasa.gov/ (files maintained by D.F. Lupishko and I.N. Belskaya)

[2] We prefer to adopt here the above classification because some classes (including the E) are no longer present in more modern taxonomic classifications, like Bus & Binzel (2002), due to the fact that purely spectroscopic data at visible wavelengths cannot distinguish among some classes of asteroids characterized by very different values of albedo, which are now all included in the modern X super-class. A more recent classification extending the wavelength coverage to the near-IR has been published by DeMeo et al. (2009), but it is still rather limited in terms of number of classified objects. In the case of the old E class, we know that it corresponds to the very high-albedo component of the modern X super-class.

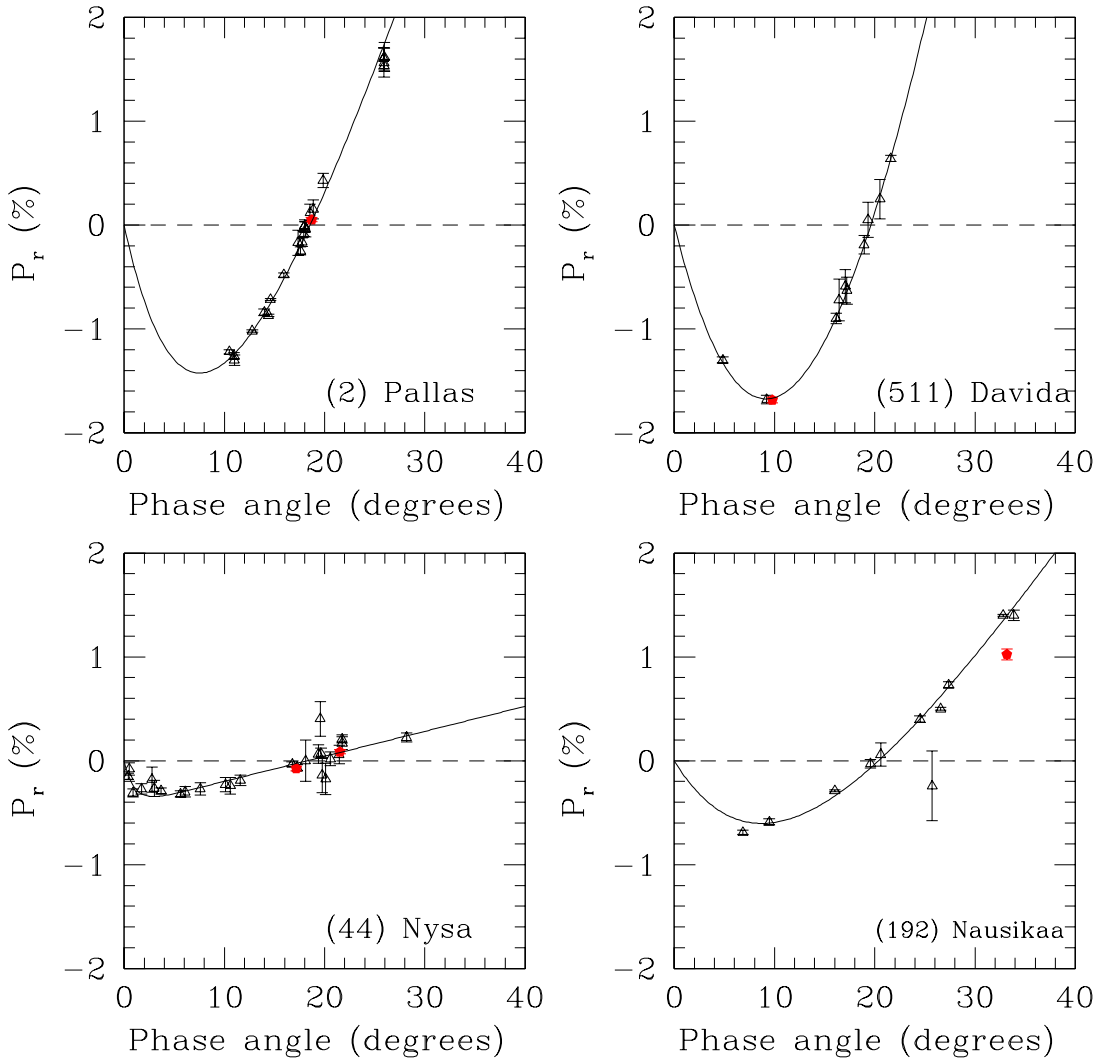

Figure 5. Phase - polarization curves for asteroids (2) Pallas, (44) Nysa , (192) Nausikaa and (511) Davida. Open symbols: data available in the literature. full symbols: new CAPS data. The best-fit curves have been computed according to Eq.14.

Also in this case, CAPS data fit nicely and extend the data available in the literature for the objects already observed in the past. As an example, we show in Fig. 7 the resulting phase-polarization curve of asteroid (51) Nemausa. In this case, some non-negligible scatter of the measurements around the best-fit curve might suggest the presence of some possible albedo heterogeneity on the surface, a possibility to be investigated in the future.

Many other taxonomic classes are already included in the CAPS database, and it is evident that one of the general goals of the CAPS survey will be to obtain a much better characterization of the polarimetric behaviour of objects belonging to different taxonomic classes, a classical task in asteroid polarimetry, in which the availability of a dedicated instrument and a significant amount of observing time is a big advantage.

The obtained results make us confident that CAPS measurements are of a very good quality (note that in Fig. 5 the nominal error bars of the CAPS data are generally smaller than the size of the symbols used in the plot), and encourage us to use them to analyze the behaviour of asteroids for which previously available polarimetric data were scarce and/or of poor quality.

Many objects in the CAPS data base were poorly observed in the past. For some of them our new data fill gaps in the existing phase - polarization curves, making it possible to improve them significantly or even to derive for the first time a reasonable fit using Eq. (14). Examples: asteroids (11), (15), (17), (23), (48), (56), (69), (71), (139), (201), (221), (236), (276), (444), (478), (679). A couple of cases are shown as an example in Fig. 8. For other objects there are only a very few published measurements, and for them CAPS data are an important addition, but still not sufficient to compute a best-fit phase - polarization curve using Eq. (14). Examples: asteroids (50), (53), (58), (59), (76), (78), (89), (94), (122), (126), (165), (185), (200), (213), (225), (306), (491),

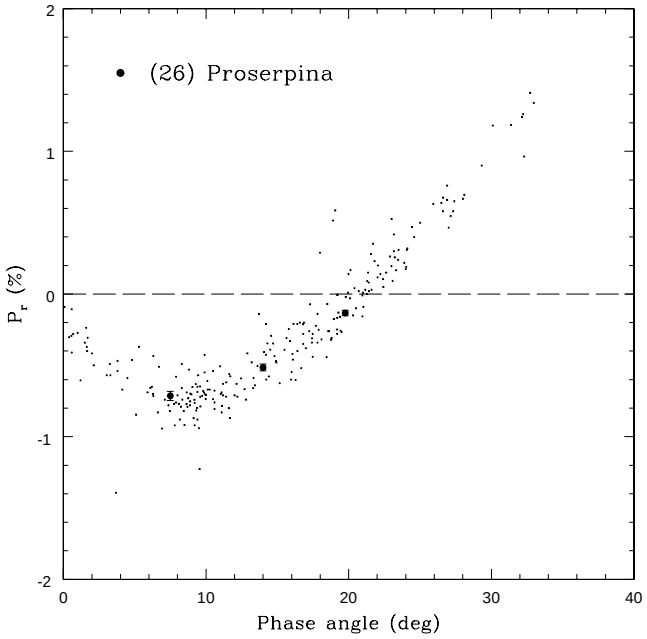

Figure 6. CAPS phase - polarization data for the *S*-class asteroid (26) Proserpina (three points shown in red colour), to be compared with all data previously available in the literature for the other asteroids belonging to this taxonomic class (small points). No previous polarimetric data had been obtained for this asteroid

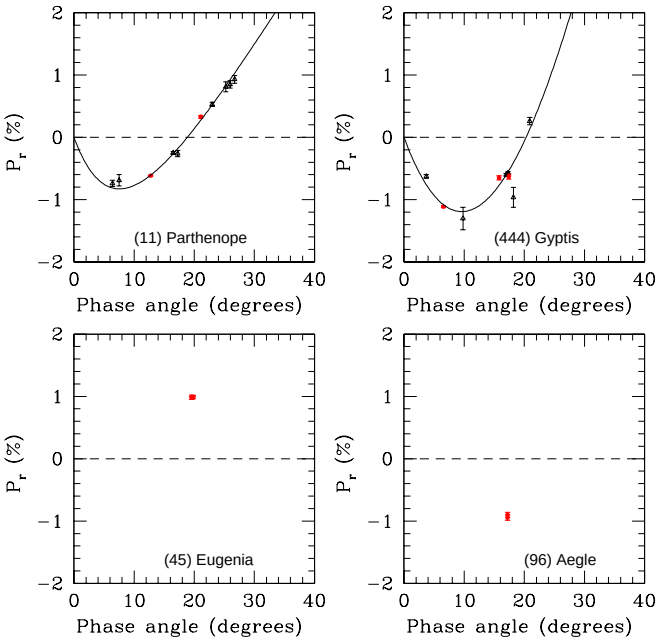

Figure 8. Phase - polarization curves for asteroids (11) Parthenope and (444) Gyptis, and new phase - polarization data for (45) Eugenia and (96) Aegle. Open symbols: data available in the literature. full symbols: new CAPS data.

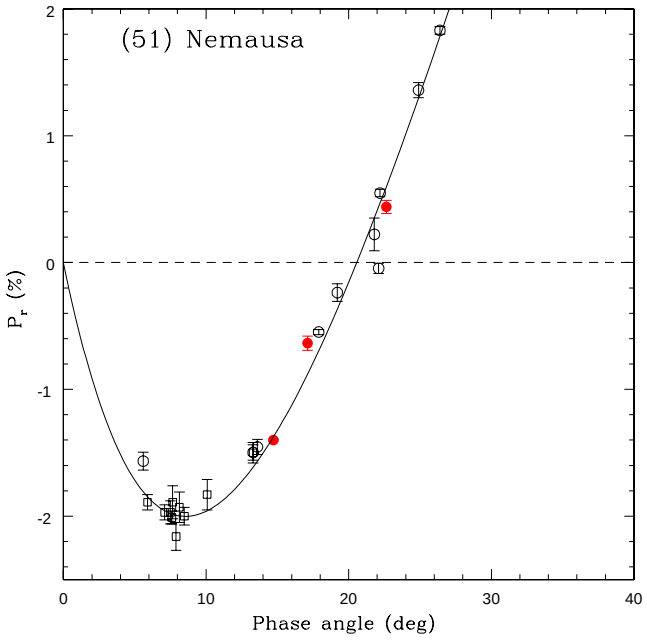

Figure 7. Phase - polarization curve of the asteroid (51) Nemausa. Open symbols: data available in the literature. Full, red symbols: new CAPS data. The best-fit curves have been computed according to Eq.14.

(532), (690), (849). The case of (532) Herculina is shown, as an example, in Fig. 9. Finally, for some objects our CAPS data are the very first existing polarimetric measurements. They are asteroids (26), (35), (38), (45), (57), (61), (96), (191), (194), (273), (304), (313), (426), (500), (783), (824), (1372), (1702) (the latter being affected by a large measurement uncertainty).

In what follows, we make a short description case-by-case of some interesting results obtained for a small number of objects of particular interest. Some of them are also shown in Figures 8, 9 and 10.

6.1 (45) Eugenia

(45) Eugenia is one of the first asteroids found to be binary systems by means of Adaptive Optics observations by Merline et al. (1999). It was classified as an *FC* class asteroid according to the Tholen classification, whereas it is classified as *C* according to the SMASS spectroscopic survey (Bus & Binzel (2002)). We have two measurements of Eugenia at a phase angle of about 20°, shown in Fig. 8. Both measurements indicate that at this phase angle, (45) Eugenia is already deeply in the positive polarization branch, suggesting a rather low value of the inversion angle. This is exactly the property characterizing the *F* class according to Belskaya et al. (2005). According to CAPS results, therefore, the most correct taxonomic classification of (45) Eugenia should be *F*. We also note that the small companion of (45) Eugenia is much fainter, and its contribution to the measured flux should be negligible.

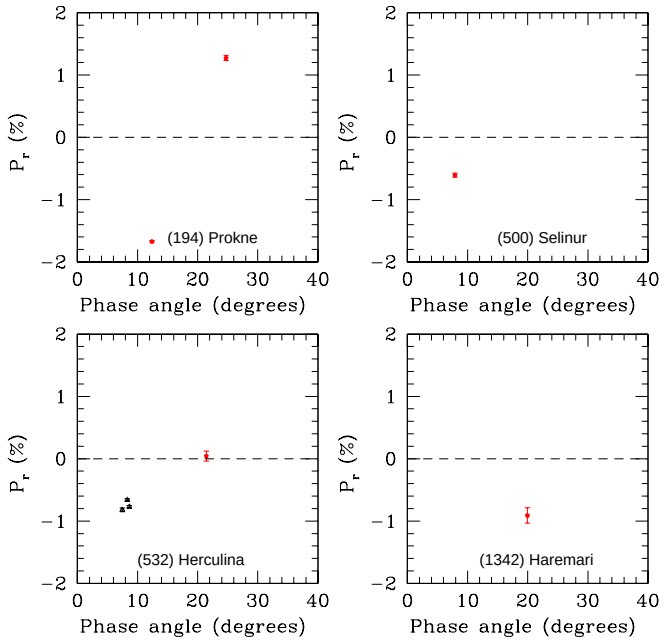

Figure 9. Phase - polarization data for asteroids (194) Prokne, (500) Selinur , (532) Herculina and (1342) Haremari. Triangles: data available in the literature for (532) Herculina. Full symbols: new CAPS data.

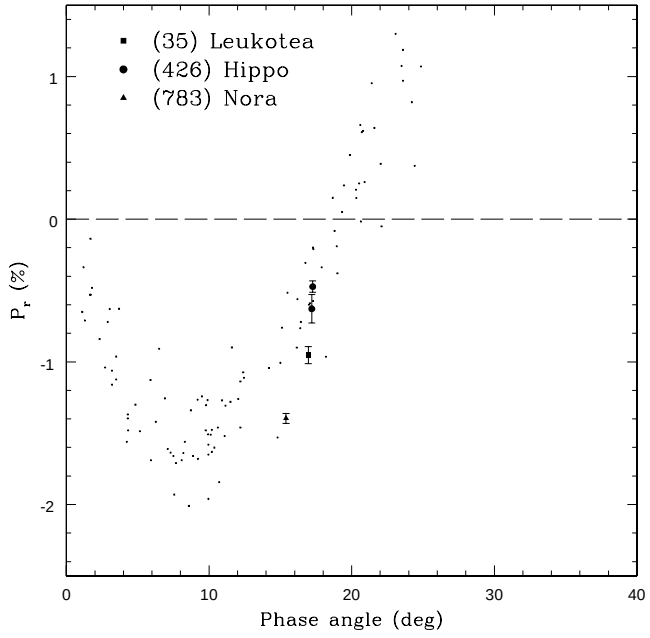

Figure 10. CAPS Phase - polarization data for asteroids (35) Leukotea, (426) Hippo and (783) Nora (large symbols), to be compared with all data available in the literature for asteroids belonging to the C taxonomic class (small points).

6.2 (96) Aegle

This asteroid is the lowest-numbered member of a dynamical family found by Milani et al. (2014). It is also classified as belonging to the rare T taxonomic class. As far as we know, our two CAPS measurements, shown in Fig. 8, are the only polarimetric data currently available for asteroids of this taxonomic class. The obtained values, obtained at a phase angle of 17°, suggest a low-albedo, and also a wide negative polarization branch. Further observations are certainly needed.

6.3 (194) Prokne

Prokne is another case of lowest-numbered member of a dynamical family identified by Milani et al. (2014). This family is located just beyond the outer border of the 3:1 mean motion resonance with Jupiter, and at a relatively high orbital inclination (sine of proper inclination about 0.3). We have obtained so far two CAPS measurements in V light for Prokne, one at a phase angle close to 12°, the other around 25°. They are shown in Fig. 9. These two measurements, though not yet sufficient to produce a fit of the phase - polarization curve by means of Eq. (14), clearly indicate that this should be a low-albedo asteroid, being characterized by a deep negative polarization branch (compare also with polarimetric data for the low-albedo C class asteroids shown as a background in Fig. 10) and confirm its C taxonomic classification (Tholen 1984). This result is also in agreement with a low-albedo value found for this object by means of thermal radiometry data obtained by the Wise satellite (Masiero et al. 2011). Note that a low albedo value for Prokne strongly suggests that this asteroid should be considered as a likely interloper in its own family, since the average albedo value of the family is higher, of the order of 0.15 according to WISE data.

6.4 (444) Gyptis

This C class asteroid has nothing special *per se*. But, because we have an excellent knowledge of its size, derived by stellar occultations, Gyptis is included in the list of asteroids with reliable values of the geometric albedo published by Shevchenko & Tedesco (2006). Several objects in this list have been recently analyzed by Cellino et al. (2015b) to derive more accurate values of the calibration coefficients appearing in differently proposed relations between geometric albedo and polarimetric properties. The new CAPS measurements, shown in Fig. 8, greatly improve the previously quite poor phase - polarization curve of Gyptis. We plan to obtain in the future a systematic improvement of the phase - polarization curves of asteroids included in the Shevchenko & Tedesco (2006) list, in a such a way as to produce further improvements in the calibration of albedo - polarization relations. This is a general example of very useful results we expect from CAPS in the field of asteroid polarimetric studies.

6.5 (500) Selinur

No taxonomic classification has been proposed so far in the literature for this asteroid. Our single value of $P_r \simeq -0.6\%$

at a phase value close to 8°, shown in Fig. 9, suggests that Selinur should have a fairly high albedo.

6.6 (1372) Haremari

(1372) Haremari is a fairly small asteroid, about 20 - 30 km in size according to different estimations based on thermal radiometry measurements by the IRAS and WISE satellites (Tedesco et al. 2002; Masiero et al. 2011). It belongs to the dynamical family of Watsonia (Novaković et al. 2011; Milani et al. 2014). This is the first family that has been found by Cellino et al. (2014) to consist of Barbarian asteroids. These objects exhibit anomalous phase - polarization curves, characterized by a very wide extension of the negative polarization branch up to values near 30°. Several Barbarians also show reflectance spectra suggesting very high abundances of the spinel mineral on their surface (Sunshine et al. 2008). Spinel is a refractory compound found in the so-called Calcium-Aluminum-rich Inclusions (CAIs) in chondritic meteorites. Barbarian asteroids might be therefore the remnants of the very first generation of planetesimals accreted in the solar system. Our single polarimetric measurement of Haremari, shown in Fig. 9, shows $P_{\rm r} = -0.911 \pm 0.124\%$ at a phase angle of 19.96°, and confirms that this asteroid must now be added to the still small list of known Barbarians.

As for other Barbarians, we note that we have obtained so far a few new polarimetric measurements also for asteroids (234) Barbara (the prototype of this class), (236) Honoria and (679) Pax. We plan to devote as much time as possible in the future to observations of these asteroids. We will present current and future CAPS data for Barbarians in a separate, dedicated paper.

6.7 A few slow rotators

Asteroids (35) Leukothea, (426) Hippo and (783) Nora are three slow rotators, with periods of 31.900 hours, 34.3 hours, and 34.4 hours, respectively. Leukothea is classified as C by different authors. For Hippo we have at disposal only an old Tholen classification as F, whereas the classification of Nora is C according to (Bus & Binzel 2002). As mentioned above, the F class, first defined by Gradie and Tedesco (1982), is characterized, in polarimetric studies, by quite low values of the inversion angle, and a correspondingly narrow extension of the negative polarization branch, as pointed out by Belskaya et al. (2005). Among our preliminary CAPS results, we have one polarimetric observation for both Leukothea and Nora, and two observations for Hippo. All these measurements are in the negative polarization branch, and are shown in Fig. 10. In all three cases, we find for these objects values of $P_{\rm r}$ which are, in some respects, slightly more negative than we could expect. In the case of (35) Leukothea and (783) Nora, we find for $P_{\rm r}$ values that are more negative (though not dramatically) with respect to usual values for most C class asteroids observed at the same phase angles. In the Fig. 10 we show for a comparison the phase - polarization curves of all C class asteroids taken from the literature. In the case of (426) Hippo, the two values of $P_{\rm r} = -0.628 \pm 0.099\%$ and $P_{\rm r} = -0.473 \pm 0.040\%$ at phase angles of 17.20° and 17.27°, respectively, are also significantly more negative than one could expect for an F class asteroid, since F objects have inversion angles around 18°, and one should expect therefore values of $P_{\rm r}$ much closer to zero at the phase angles of our observations of Hippo. On the other hand, our two measurements of Hippo show also a steep increase, which suggests a fast "race" to the inversion angle. Of course, further observations are needed for all three objects, and we cannot rule out a priori the possibility that the F classification of Hippo could be wrong. It is interesting to note, however, that all the three objects are slow rotators. This may be just a coincidence, but we know that several Barbarian asteroids, which exhibit values of $P_{\rm r}$ more negative than normal in a wide range of phase angles, are also known to be slow rotators, as in the cases of (234) Barbara and (1372) Haremari, whose spin periods are longer than 15 hours. It is difficult to imagine a possible direct relation between slow rotation and unusual polarization properties. However, we cannot rule out the possibility that both the rotation state and surface properties might depend on the age. The hypothesis of a relation between slow rotation and polarimetric properties is something that can be explored by carrying out a dedicated telescope survey like CAPS.

7 CONCLUSIONS

We can summarize briefly the results obtained in the present analysis.

(i) The ToPol is characterized by a comparatively high, but stable instrumental polarization.

(ii) The results so far obtained for asteroids are in agreement with those previously published in the literature. In the case of poorly observed asteroids, CAPS measurements are already useful to improve significantly the coverage in phase angle. Many of these objects can be used to calibrate the relations between geometric albedo and polarimetric properties.

(iii) In a number of cases, the very preliminary results obtained so far are important since they concern objects which are particularly interesting due to rare taxonomic classifications, family membership, unusual rotation rates and/or peculiar polarimetric properties (Barbarian asteroids).

(iv) By carrying out our Calern Asteroid Polarimetric Survey we expect to be able to improve significantly the data set of asteroid polarization data, and to explore systematically some interesting branches of research, including Barbarians and a possible relation between slow rotation and unusual polarization properties, to be possibly interpreted in terms of evolutionary processes.

Based on the preliminary results presented in this paper, we are convinced that the Calern Asteroid Polarization Survey can play an important role for asteroid studies in the years to come. Moreover, we also plan to use the new polarimeter to perform polarimetric studies of other solar system bodies, including major planets and the Moon. Some preliminary results we have already obtained will be published in separate papers.

ACKNOWLEDGEMENTS

The Torino polarimeter was built at the INAF - Torino Astrophysical Observatory and funded by INAF in the framework of INAF PRIN 2009.

Part of this work by MD was supported by the COST Action MP1104 "Polarization as a tool to study the Solar System and beyond".

The authors express their gratitude to the technical and administrative staff of the Calern observing station for their help and kind support.

REFERENCES

Bagnulo, S., Cellino, A., & Sterzik, M. F. 2015, MNRAS, 446, L11

Bagnulo, S., Belskaya, I., Boehnhardt, H., Kolokolova, L., Muinonen, K.,Sterzik, M., Tozzi, G.-P., 2011, JQSRT, 112, 2059

Bagnulo, S., Boehnhardt H., Muinonen K., Kolokolova L., Belskaya I., Barucci M. A., 2006, A&A, 450, 1239

Bailey, J., Hough J., 1982, Publications of the Astronomical Society of the Pacific, 94, 618

Bastien, P., Vernet, E., Drissen, L., Menard, F., Moffat A.F.J., Robert, C., St-Louis, N. 2007, ASP Conference Series, 364, 529

Bastien, P., Drissen, L., Menard, F., Moffat A.F.J., Robert, C., St-Louis, N. 2007, The Astronomical Journal, 95, 900

Belskaya, I.N. et al, 2005, Icarus, 178, 213

Belskaya, I.N. et al, 2015, in Asteroids IV, Ed. P. Michel, F. DeMeo, & W.F. Bottke, Univ. of Arizona Press, Tucson, 151

Bus, S., & Binzel, R.P. 2002, Icarus, 158, 146

Cellino A., Belskaya I. N., Bendjoya Ph., di Martino M., Gil-Hutton R., Muinonen K., Tedesco E. F., Icarus, 180, 565

Cellino, A., Gil-Hutton, R., Belskaya, I. N. 2015a, in Polarimetry of Stars and Planetary Systems, Ed. L. Kolokolova, J. Hough, & A.-C. Levasseur-Regourd (Cambridge University Press) 360

Cellino, A., Bagnulo, S., Gil-Hutton, R., Tanga, P., Caãda-assandri, M., Tedesco, E. F. 2015b, MNRAS, 451, 3473

Cellino, A., Bagnulo, S., Gil-Hutton, R., Tanga, P., Caãda-assandri, M., Tedesco, E. F. 2016, MNRAS, 455, 2091

Cellino, A., Bagnulo, S., Tanga, P., Novaković, B., Delbò, M. 2014, MNRAS, 439, L75

Clemens, D., Tapia S., 1990, Astronomical Society of the Pacific, 102, 179

DeMeo, F. E., Binzel, R. P., Slivan, S. M., Bus, S. J., 2009, Icarus, 202, 160

Devogèle 2015, European Planetary Science Congress 2015, EPSC2015-469

Dollfus, A. Wolff, M., Geake, J.E., Lupishko, D.F., & Dougherty, L., 1989, in Asteroids II, Ed. R.P. Binzel, T. Gehrels, & M.S. Matthews, Univ. of Arizona Press, Tucson, 594

Fornasier, S., Belskaya I.N., Shkuratov Yu. G., Pernechele C., Barbieri C., Giro E., Navasardyan H., 2006, A&A, 455, 371

Fornasier, S., Belskaya I.N., Perna, D., 2015, Icarus, 250, 280

Gil Hutton, R., Cellino, A., Bendjoya, Ph. 2014, A&A, 569, A122

Gil Hutton, R., Caada-Assandri M., 2012, A&A, 539, A115

Gradie, J., Tedesco, E. F. 1982, Science, 216, 1405

Gehrels, T. 1974, University of Arizona Press, Tuscon, 168

Hsu, J.-C., Breger, M., 1982 182, Astrophysical Journal, 262, 732

Hiltner, W.A. 1951, Astron. J., 114, 241

International Astronomical Union, 1973,Transactions of the IAU Vol. 15B,166

Masiero J., et al. 2011, The Astrophysical Journal, 741, 68

Merline, W. et al. 1999, Nature, 401, 565

Milani, A., Cellino, A., Knežević, Z., Novaković, B., Spoto, F., Paolicchi, P., 2014, Icarus, 239, 46

Muinonen et al., 2009, Meteoritics and Planet. Sci., 44, 1937

Novaković, B., Cellino, A., & Knežević, Z. 2011, Icarus, 216, 69

Oliva, E. (1997) A&ASS, 123, 589

Pernechele, C., Abe, L., Bendjoya, Ph., Cellino, A., Massone, G., Tanga, P. 2012, Proceedings of the SPIE, 8446, 84462H

Petrova E.V., Tishkovets V. P., Jockers K., 2004, Solar System Research, 38, 354

Schmidt, G., Elston R., 1992, The Astronomical Journal, 104, 1563

Schulz, A., Lenzen, R., 1983, Astro. Astrophys. Research Note, 121, 158

Shurcliff, W.A., 1962, Polarized Light (Mass: Harward University Press, Cambridge)

Shevchenko, V.G., & Tedesco, E.F. 2006. Icarus,184, 211-220

Sunshine, J., Connolly, H.C., Mc Coy, Bus, S.J., La Croix, L.M. 2008, Science, 320, 514

Tedesco, E.F., Noah, P.V., Noah, M., Price, S.D. 2005, The Astronomical Journal, 123, 1056

Tholen, D.J. 1984, "Asteroid Taxonomy from Cluster Analysis of Photometry". PhD thesis, University of Arizona.

Turnshek, D. A., Bohlin, R. C., Williamson, R. L., II, Lupie, O. L., Koornneef, J., Morgan, D. H., 1990, Astronomical Journal, 99, 1243

Wolff, M., Nordsieck, K., Nook, M., 1996, The Astronomical Journal, 111, 856

Wilking, B., Lobokski, M., Martin, P., Rieke G., Kemp, K., 1980, The Astronomical Journal, 235, 905

Zellner, B. & Gradie, J., 1976, The Astronomical Journal, 81, 262

APPENDIX A: TABLE OF THE OBSERVATION OF STANDARD CALIBRATION STARS

APPENDIX B: TABLE OF CURRENTLY AVAILABLE CAPS DATA

Star	Filter	Mag	Obs date	$N_{\rm obs}$	$t_{\rm exp}$ [s]	q_0	σ_{q_0}	u_0	σ_{u_0}
HD10476	V	5.24	2015/10/14	91	0.5	3.801×10^{-2}	7.5×10^{-5}	-4.723×10^{-3}	8.3×10^{-5}
HD10476	V	5.24	2015/10/15	30	1	3.773×10^{-2}	7.3×10^{-5}	-4.542×10^{-3}	8.8×10^{-5}
HD10476	V	5.24	2015/12/08	34	0.2	3.756×10^{-2}	1.2×10^{-4}	-6.643×10^{-3}	8.5×10^{-5}
HD10476	V	5.24	2015/12/09	30	0.1	3.778×10^{-2}	1.6×10^{-4}	-5.342×10^{-3}	1.5×10^{-4}
HD10476	V	5.24	2015/12/10	30	0.1	3.734×10^{-2}	2.2×10^{-4}	-7.334×10^{-3}	1.2×10^{-4}
HD10476	V	5.24	2015/12/11	30	0.5	3.742×10^{-2}	5.3×10^{-4}	-6.437×10^{-3}	1.3×10^{-4}
HD18803	V	6.62	2015/02/19	20	0.5	3.834×10^{-2}	1.8×10^{-4}	-3.71×10^{-3}	3.7×10^{-4}
HD18803	R	6.2	2015/02/19	24	0.5	3.642×10^{-2}	1.5×10^{-4}	-2.72×10^{-3}	1.6×10^{-4}
HD18803	V	6.62	2015/10/15	20	2	3.754×10^{-2}	8.3×10^{-5}	-4.432×10^{-3}	8.2×10^{-5}
HD18803	V	6.62	2015/12/10	31	0.5	3.723×10^{-2}	2.3×10^{-4}	-5.290×10^{-3}	1.8×10^{-4}
HD20630	V	4.85	2015/02/19	41	0.1	3.872×10^{-2}	1.9×10^{-4}	-4.58×10^{-3}	3.2×10^{-4}
HD20630	R	4.27	2015/02/19	20	0.1	3.654×10^{-2}	1.4×10^{-4}	-3.32×10^{-3}	2.1×10^{-4}
HD20630	V	4.85	2015/02/22	23	1	3.792×10^{-2}	1.2×10^{-4}	-2.58×10^{-3}	8.5×10^{-5}
HD20630	R	4.27	2015/02/22	21	1	3.613×10^{-2}	1.3×10^{-4}	-2.34×10^{-3}	6.3×10^{-4}
HD39587	V	4.40	2015/02/22	46	0.2	3.897×10^{-2}	1.3×10^{-4}	-2.39×10^{-3}	1.4×10^{-4}
HD39587	R	3.9	2015/02/22	24	0.2	3.667×10^{-2}	1.5×10^{-4}	-2.90×10^{-3}	8×10^{-4}
HD39587	V	4.40	2015/10/16	30	0.05	3.881×10^{-2}	6.8×10^{-5}	-1.82×10^{-3}	7.9×10^{-5}
HD39587	V	4.40	2015/12/11	30	0.2	3.813×10^{-2}	1.3×10^{-4}	-5.32×10^{-3}	1.8×10^{-4}
HD42807	V	6.44	2015/02/18	22	0.5	3.751×10^{-2}	1.4×10^{-4}	-2.61×10^{-3}	1.8×10^{-4}
HD42807	R	6.0	2015/02/18	21	0.5	3.584×10^{-2}	1.4×10^{-4}	-3.00×10^{-3}	1.7×10^{-4}
HD42807	V	6.44	2015/02/22	21	0.5	3.836×10^{-2}	1.8×10^{-4}	-3.11×10^{-3}	3.2×10^{-4}
HD42807	R	6.0	2015/02/22	20	0.5	3.700×10^{-2}	$1.4. \times 10^{-4}$	-2.58×10^{-3}	1.9×10^{-4}
HD42807	V	6.44	2015/12/09	30	1	3.731×10^{-2}	1.4×10^{-4}	-3.431×10^{-3}	1.1×10^{-4}
HD65583	V	7.00	2015/02/18	20	1	3.810×10^{-2}	2.8×10^{-4}	-3.34×10^{-3}	2.1×10^{-4}
HD65583	R	6.4	2015/02/18	20	1	3.661×10^{-2}	1.8×10^{-4}	-3.01×10^{-3}	2.1×10^{-4}
HD65583	V	7.00	2015/02/22	20	0.5	3.826×10^{-2}	1.8×10^{-4}	-2.16×10^{-3}	2.6×10^{-4}
HD65583	R	6.4	2015/02/22	23	0.5	3.631×10^{-2}	2.4×10^{-4}	-2.42×10^{-3}	2.3×10^{-4}
HD65583	V	7.00	2015/02/25	200	1	3.796×10^{-2}	5.5×10^{-5}	-2.69×10^{-3}	6×10^{-5}
HD65583	R	6.4	2015/02/25	200	1	3.623×10^{-2}	4.2×10^{-5}	-2.25×10^{-3}	7.5×10^{-5}
HD90508	R	5.98	2015/02/18	20	0.5	3.612×10^{-2}	2.2×10^{-4}	-3.25×10^{-3}	1.5×10^{-4}
HD90508	V	6.45	2015/02/22	20	0.5	3.845×10^{-2}	1.8×10^{-4}	-2.25×10^{-3}	2.5×10^{-4}
HD90508	R	5.98	2015/02/22	20	0.5	3.591×10^{-2}	$1.6. \times 10^{-4}$	-1.71×10^{-3}	1.5×10^{-4}
HD90508	V	6.45	2015/03/03	650	1	3.8495×10^{-2}	5.1×10^{-5}	-2.72×10^{-3}	1.2×10^{-4}
HD90508	V	6.45	2015/03/05	4800	1	3.8362×10^{-2}	$1.1. \times 10^{-5}$	-2.352×10^{-3}	1.0×10^{-5}
HD90508	V	6.45	2015/03/07	2500	1	3.7747×10^{-2}	1.4×10^{-5}	-2.847×10^{-3}	1.0×10^{-5}
HD90508	V	6.45	2015/03/28	50	1.5	3.827×10^{-2}	8×10^{-5}	-2.584×10^{-3}	7×10^{-5}
HD90508	V	6.45	2015/03/30	1100	1	3.8570×10^{-2}	2.3×10^{-5}	-3.085×10^{-3}	2.5×10^{-5}
HD90508	V	6.45	2015/12/10	20	1	3.7542×10^{-2}	1.4×10^{-4}	-7.4727×10^{-3}	3.7×10^{-4}
HD90508	V	6.45	2015/12/11	32	1	3.787×10^{-2}	1.4×10^{-4}	-7.7529×10^{-3}	2.6×10^{-4}
HD98281	V	7.23	2015/02/22	20	2	3.828×10^{-2}	1.4×10^{-4}	-2.40×10^{-3}	1.7×10^{-4}
HD98281	R	6.82	2015/02/22	20	2	3.640×10^{-2}	9×10^{-5}	-1.9×10^{-3}	1.3×10^{-4}
HD103095	V	6.45	2015/02/22	24	0.5	3.788×10^{-2}	2.3×10^{-4}	-2.245×10^{-3}	1.1×10^{-4}
HD103095	R	5.80	2015/02/22	20	0.5	3.645×10^{-2}	8.2×10^{-5}	-2.84×10^{-3}	1.5×10^{-4}
HD103095	V	6.45	2015/03/27	150	2	3.821×10^{-2}	1.1×10^{-4}	-3.388×10^{-3}	9.3×10^{-5}
HD103095	V	6.45	2015/03/28	230	1.5	3.835×10^{-2}	7.3×10^{-5}	-3.064×10^{-3}	6.5×10^{-5}
HD114710	V	3.25	2015/02/22	20	0.1	3.850×10^{-2}	1.1×10^{-4}	-5.34×10^{-3}	2.2×10^{-4}
HD114710	R	3.77	2015/02/22	20	0.1	3.606×10^{-2}	1.5×10^{-4}	-4.23×10^{-3}	1.1×10^{-4}
HD114710	V	3.25	2015/02/25	100	0.1	3.8350×10^{-2}	3.6×10^{-5}	-4.86×10^{-3}	1.1×10^{-4}
HD114710	R	3.77	2015/02/25	100	0.1	3.604×10^{-2}	7×10^{-5}	-3.330×10^{-3}	9×10^{-5}
HD142373	V	4.62	2015/02/22	21	0.1	4.000×10^{-2}	1.4×10^{-4}	-4.32×10^{-3}	2.2×10^{-4}
HD142373	R	4.14	2015/02/22	20	0.1	3.732×10^{-2}	1.8×10^{-4}	-4.60×10^{-3}	1.5×10^{-4}
HD142373	V	4.62	2015/02/25	100	0.5	3.8226×10^{-2}	3.6×10^{-5}	-2.468×10^{-3}	5.5×10^{-5}
HD154345	V	6.74	2015/07/17	30	1	3.876×10^{-2}	1.2×10^{-4}	-3.220×10^{-3}	1.6×10^{-4}
HD154345	V	6.74	2015/07/23	30	1	3.776×10^{-2}	2.0×10^{-4}	-3.356×10^{-3}	1.7×10^{-4}
HD165908	V	5.07	2015/07/17	30	0.1	3.920×10^{-2}	1.4×10^{-4}	-3.565×10^{-3}	1.4×10^{-4}
HD165908	V	5.07	2015/07/18	30	0.1	3.960×10^{-2}	5.4×10^{-4}	-3.375×10^{-3}	2.9×10^{-4}
HD165908	V	5.07	2015/07/23	30	0.1	3.881×10^{-2}	1.7×10^{-4}	-5.503×10^{-3}	1.6×10^{-4}
HD185395	V	4.48	2015/07/13	30	0.1	3.892×10^{-2}	2.6×10^{-4}	-5.840×10^{-3}	3.2×10^{-4}
HD185395	V	4.48	2015/07/14	30	0.1	3.861×10^{-2}	2.3×10^{-4}	-5.871×10^{-3}	2.2×10^{-4}
HD185395	V	4.48	2015/07/15	30	0.1	3.860×10^{-2}	3.4×10^{-4}	-4.783×10^{-3}	6.4×10^{-4}
HD185395	V	4.48	2015/07/18	30	0.1	3.935×10^{-2}	2.2×10^{-4}	-4.321×10^{-3}	6.7×10^{-4}
HD185395	V	4.48	2015/07/21	30	0.1	3.967×10^{-2}	5.0×10^{-4}	-4.835×10^{-3}	2.2×10^{-4}
HD188512	V	3.71	2015/07/21	30	0.03	3.883×10^{-2}	1.2×10^{-4}	-4.731×10^{-3}	2.1×10^{-5}
HD210027	V	3.77	2015/07/16	30	0.05	4.009×10^{-2}	3.5×10^{-4}	-5.036×10^{-3}	1.1×10^{-5}
HD202573	V	6.98	2015/07/16	30	1	3.783×10^{-2}	3.8×10^{-4}	-3.343×10^{-3}	2.1×10^{-5}

Table A1. Summary table of all observations for unpolarized standard stars. The first column corresponds to the name of the star. The second column gives the magnitude in the respective filter. $N_{\rm obs}$ represents the number of observed frames, $t_{\rm exp}$ is the exposure time of the individual frames, q_0 is the measured instrumental q reduced Stokes parameter, σ_{q_0} is the error bar associated to q_0, u_0 is the measured instrumental u reduced Stokes parameter and σ_{u_0} is the error bar associated to u_0.

Star	Filter	Mag	Obs date	$N_{\rm obs}$	$t_{\rm exp}$ [s]	q_0	σ_{q_0}	u_0	σ_{u_0}
HD144287	V	7.06	2015/02/18	19	1	3.757×10^{-2}	1.6×10^{-4}	-3.25×10^{-3}	1.2×10^{-4}
HD144287	R	7.06	2015/02/18	22	1	3.656×10^{-2}	1.6×10^{-4}	-3.07×10^{-3}	1.3×10^{-4}
HD144287	V	7.06	2015/02/22	20	1	3.580×10^{-2}	2.6×10^{-4}	-2.65×10^{-3}	1.4×10^{-4}
HD144287	R	7.06	2015/02/22	20	1	3.477×10^{-2}	2.2×10^{-4}	-3.82×10^{-3}	2.7×10^{-4}
HD144287	V	7.06	2015/02/25	100	1	3.7966×10^{-2}	8×10^{-5}	-2.561×10^{-3}	8×10^{-5}
HD144579	V	6.67	2015/02/22	20	0.5	3.837×10^{-2}	2.2×10^{-4}	-2.85×10^{-3}	2.3×10^{-4}
HD144579	R	6.04	2015/02/22	20	0.5	3.636×10^{-2}	2.0×10^{-4}	-3.00×10^{-3}	2.0×10^{-4}
HD202573	V	6.98	2015/11/15	30	2.5	3.7219×10^{-2}	7.9×10^{-4}	-4.6623×10^{-3}	8.5×10^{-5}
HD202573	V	6.98	2015/12/08	31	0.5	3.8143×10^{-2}	1.7×10^{-4}	-5.5807×10^{-3}	2.3×10^{-4}
HD202573	V	6.98	2015/12/10	30	1	3.7598×10^{-2}	1.5×10^{-4}	-5.8271×10^{-3}	1.4×10^{-4}
HD202573	V	6.98	2015/12/11	30	1	3.6713×10^{-2}	1.9×10^{-4}	-6.093×10^{-3}	1.8×10^{-4}

Table A2. Summary table of all observations for unpolarized standard stars. Continued table.

Star	Filter	Mag	Obs date	$N_{\rm obs}$	$t_{\rm exp}$ [s]	P [$\times 10^{-2}$]	O-C(P) [$\times 10^{-2}$]	θ [Deg]	O-C(θ) [Deg]
HD14433	V	6.39	2015/02/19	23	1	3.82 ± 0.10	-0.05	111.4 ± 0.7	-1.1
HD14433	R	5.79	2015/02/19	23	1	3.66 ± 0.09	-0.03	111.7 ± 0.6	-0.3
HD14433	V	6.39	2015/02/22	20	1	4.03 ± 0.02	0.15	112.8 ± 0.2	0.3
HD14433	R	5.79	2015/02/22	22	1	3.72 ± 0.03	0.03	113.1 ± 0.2	1
HD23512	V	8.09	2015/02/19	20	5	2.29 ± 0.10	0.08	27.5 ± 0.7	-0.6
HD23512	R	7.79	2015/02/19	20	5	2.14 ± 0.09	0.06	27.6 ± 0.6	-2
HD43384	V	6.25	2015/02/18	60	0.5	2.97 ± 0.04	0.12	170.0 ± 0.3	2.6
HD43384	R	5.78	2015/02/18	60	0.5	2.89 ± 0.04	0.09	170.3 ± 0.3	0.5
HD43384	V	6.25	2015/10/16	60	0.5	2.75 ± 0.02	-0.10	171.0 ± 0.2	3.6
HD43384	V	6.25	2015/12/09	60	0.5	2.85 ± 0.04	0	169.7 ± 0.3	1.3
HD43384	V	6.25	2015/12/11	60	0.5	2.89 ± 0.05	0.04	170.0 ± 0.4	2.6
HD154445	V	5.61	2015/02/18	20	0.2	3.67 ± -0.05	0.03	89.1 ± 0.2	-0.6
HD154445	R	5.39	2015/02/18	20	0.2	3.72 ± 0.05	0.29	88.9 ± 0.3	0.2
HD154445	V	5.61	2015/02/25	20	1	3.74 ± 0.1	0.02	89.0 ± 0.2	-0.7
HD154445	V	5.61	2015/03/27	40	1	3.66 ± 0.03	-0.06	88.5 ± 0.2	-1.2
HD154445	V	5.61	2015/05/12	30	1	3.72 ± 0.02	0	88.8 ± 0.2	-0.7
HD154445	V	5.61	2015/07/23	30	1	3.68 ± 0.06	-0.04	88.3 ± 0.5	-1.4
HD183143	V	6.86	2015/07/14	30	1	6.03 ± 0.06	0.09	0.2 ± 0.3	0.3
HD183143	V	6.86	2015/07/17	30	1	5.94 ± 0.03	0.00	178.8 ± 0.2	-1.1
HD183143	V	6.86	2015/07/18	30	1	5.92 ± 0.04	-0.02	179.3 ± 0.2	-0.6
HD187929	V	3.80	2015/07/13	30	0.1	1.77 ± 0.04	0.01	92.3 ± 0.5	0.3
HD187929	V	3.80	2015/07/15	30	0.1	1.63 ± 0.04	-0.13	92.8 ± 0.4	0.8
HD198478	V	4.86	2015/07/21	30	0.5	2.68 ± 0.05	-0.01	2.0 ± 0.7	-3.1
HD204827	V	7.94	2015/07/16	30	2	5.62 ± 0.06	0.21	58.7 ± 0.3	-0.3
HD251204	V	10.2	2015/02/18	20	10	4.98 ± 0.03	0.63	163.2 ± 0.3	12.1

Table A3. Summary table of all observations for polarized standard stars. The first column correspond to the name of the star. The second column reports the magnitude in the respective filter. $N_{\rm obs}$ represents the number of observed frames, $t_{\rm exp}$ is the exposure time of the individual frames, P is the measured linear polarization (after correction for the instrumental polarization), O-C(P) is the difference between the observed and the expected linear polarization from reference sources, θ is the measured polarization angle with respect to the North direction and O-C(θ) is the difference between the observed and the expected polarization angles from reference sources

Star	Filter	Mag	P [$\times 10^{-2}$]	θ [Deg]	References
HD14433	V	6.39	3.87 ± 0.01	112.5 ± 0.1	Hsu and Breger (1982)
HD14433	R	5.79	3.69 ± 0.01	112.4	Hsu and Breger (1982)
HD23512	V	8.09	2.21 ± 0.02	28.1 ± 1.2	Hsu and Breger (1982); Bastien et al. (1988)
HD23512	R	7.79	2.20 ± 0.02	29.6 ± 1.2	Hsu and Breger (1982)
HD43384	V	6.25	2.85 ± 0.10	168.4 ± 1.4	Hsu and Breger (1982)
HD43384	R	5.78	2.80 ± 0.03	169.8 ± 0.9	Hsu and Breger (1982)
HD154445	V	5.61	3.72 ± 0.02	89.5 ± 0.4	Hsu and Breger (1982); Bastien et al. (1988) Turnshek et al. (1990); Schmidt (1992)
HD154445	R	5.39	3.43 ± 0.16	89.7 ± 0.4	Hsu and Breger (1982); Schmidt (1992)
HD183143	V	6.86	5.94 ± 0.13	179.9	Schulz (1983); Bailey & Hough. (1982) Clemens & Tapia (1990)
HD187929	V	3.80	1.76 ± 0.04	92.0 ± 0.7	Bastien et al. (1988); Bailey & Hough. (1982)
HD198478	V	4.86	2.69 ± 0.07	5.1	Hsu and Breger (1982)
HD204827	V	7.94	5.41 ± 0.08	59.0 ± 0.3	Schulz (1983); Bastien et al. (1988)
HD251204	V	10.2	4.37 ± 0.33	151 ± 0.4	Turnshek et al. (1990); Hitlner (1951)

Table A4. References for the polarized standard stars which were observed. The degree of polarization and polarization angle correspond to the mean value of all reported values in the literature.

Table B1. Summary table of all the asteroids observed by the CAPS survey. The first column correspond to the number of the asteroid, the second column stand for the date of observation. α stand for the phase angle during the observation, P_r is the linear polarization degree and the last column represent the filter used.

Object Number	Date	α [Deg]	P_r [%]	Filter
2	2015/02/18	18.70	0.052 ± 0.032	V
2	2015/02/18	18.70	0.081 ± 0.039	R
3	2015/02/18	11.91	-0.658 ± 0.022	V
3	2015/02/18	11.91	-0.645 ± 0.019	R
6	2015/02/19	27.14	0.463 ± 0.035	V
6	2015/02/19	27.14	0.453 ± 0.038	R
7	2015/02/18	8.24	-0.635 ± 0.026	V
7	2015/02/18	8.24	-0.825 ± 0.030	R
8	2015/02/18	3.33	-0.468 ± 0.025	V
8	2015/02/18	3.33	-0.593 ± 0.022	R
8	2015/03/11	12.40	-0.320 ± 0.025	V
10	2015/02/18	14.45	-0.790 ± 0.030	V
10	2015/02/18	14.45	-0.776 ± 0.045	R
11	2015/02/18	21.08	0.251 ± 0.028	V
11	2015/02/18	21.08	0.151 ± 0.025	R
11	2015/05/20	12.75	-0.642 ± 0.024	V
15	2015/07/15	26.05	0.391 ± 0.054	V
17	2015/02/18	8.14	-0.710 ± 0.033	V
17	2015/02/18	8.14	-0.707 ± 0.024	R
18	2015/02/19	20.25	-0.283 ± 0.047	V
18	2015/02/19	20.25	0.244 ± 0.052	R
20	2015/02/19	22.38	0.247 ± 0.048	V
20	2015/02/19	22.38	0.176 ± 0.043	R
23	2015/02/19	28.37	0.616 ± 0.031	V
23	2015/02/19	28.37	0.757 ± 0.034	R
25	2015/02/22	20.15	0.157 ± 0.039	R
26	2015/10/15	14.00	-0.515 ± 0.023	V
29	2015/10/15	5.33	-0.802 ± 0.010	V
35	2015/02/18	16.96	-1.170 ± 0.069	V
38	2015/02/18	2.74	-1.016 ± 0.033	V
38	2015/02/18	2.74	-0.998 ± 0.038	R
42	2015/02/18	8.09	-0.638 ± 0.029	V
42	2015/02/18	8.09	-0.679 ± 0.034	R
43	2015/10/15	16.10	-0.270 ± 0.022	V
44	2015/02/18	17.17	-0.033 ± 0.031	V
44	2015/02/18	17.17	-0.020 ± 0.025	R
44	2015/05/13	21.53	0.063 ± 0.032	V
45	2015/07/15	19.84	1.009 ± 0.105	V
45	2015/07/17	19.54	0.983 ± 0.029	V
48	2015/07/13	12.83	-2.035 ± 0.052	V
48	2015/07/14	13.04	-1.923 ± 0.053	V
50	2015/02/18	12.96	-1.656 ± 0.051	V
51	2015/05/12	14.72	-1.342 ± 0.021	V
51	2015/07/14	17.12	-0.673 ± 0.060	V
51	2015/10/14	22.64	0.439 ± 0.052	V
53	2015/02/19	19.32	-0.298 ± 0.050	V
53	2015/02/19	19.32	-0.369 ± 0.045	R
56	2015/02/19	6.39	-0.918 ± 0.068	V
56	2015/02/19	6.39	-1.128 ± 0.045	R
57	2015/07/14	7.01	-0.758 ± 0.057	V
57	2015/07/15	6.90	-0.801 ± 0.047	V
58	2015/02/22	6.05	-0.861 ± 0.022	V
59	2015/05/12	7.67	-1.134 ± 0.027	V
61	2015/07/22	23.83	0.327 ± 0.047	V
69	2015/02/19	15.64	-0.795 ± 0.026	V
69	2015/02/19	15.64	-0.769 ± 0.034	R
69	2015/05/21	21.95	0.242 ± 0.023	V
71	2015/02/19	7.64	-0.500 ± 0.031	V
71	2015/02/19	7.64	-0.420 ± 0.047	R
76	2015/02/19	3.23	-0.545 ± 0.045	V
76	2015/02/19	3.23	-0.664 ± 0.034	R

Table B2. The current CAPS data set (continued)

Object number	Date	α [Deg]	P_r [%]	Filter
78	2015/03/07	24.82	0.940 ± 0.056	V
86	2015/02/19	6.27	-1.389 ± 0.076	V
86	2015/02/19	6.27	-1.239 ± 0.053	R
89	2015/02/19	6.09	-0.808 ± 0.025	V
89	2015/02/19	6.09	-0.821 ± 0.034	R
94	2015/02/22	16.63	-0.397 ± 0.034	V
96	2015/07/21	17.22	-0.916 ± 0.055	V
96	2015/07/23	17.22	-0.841 ± 0.055	V
103	2015/10/10	13.70	-0.494 ± 0.026	V
122	2015/05/20	3.07	-0.453 ± 0.037	V
122	2015/05/22	3.45	-0.513 ± 0.031	V
126	2015/02/22	4.20	-0.690 ± 0.025	V
128	2015/02/22	9.27	-1.507 ± 0.019	R
133	2015/02/22	15.78	-0.468 ± 0.069	R
139	2015/03/28	23.05	0.810 ± 0.029	V
165	2015/07/16	19.59	0.078 ± 0.060	V
168	2015/02/22	12.94	-1.752 ± 0.036	R
185	2015/07/16	18.56	-0.008 ± 0.056	V
191	2015/07/16	12.89	-0.902 ± 0.056	V
192	2015/07/16	33.18	1.023 ± 0.050	V
194	2015/05/21	12.40	-1.692 ± 0.025	V
194	2015/07/17	24.72	1.295 ± 0.036	V
200	2015/07/22	13.40	-1.725 ± 0.043	V
200	2015/10/15	19.25	-0.596 ± 0.022	V
201	2015/07/14	23.55	0.276 ± 0.058	V
201	2015/07/15	23.35	0.183 ± 0.056	V
213	2015/10/16	17.30	-0.352 ± 0.026	V
221	2015/07/14	17.78	-0.587 ± 0.056	V
225	2015/10/16	13.83	-0.735 ± 0.024	V
234	2015/02/25	16.95	-1.512 ± 0.047	V
234	2015/05/22	17.38	-1.424 ± 0.023	V
236	2015/02/22	11.50	-1.285 ± 0.065	V
236	2015/03/30	0.41	0.021 ± 0.035	V
236	2015/05/21	15.26	-1.232 ± 0.045	V
273	2015/07/23	17.87	-0.345 ± 0.058	V
276	2015/07/23	15.74	-0.305 ± 0.045	V
304	2015/07/17	19.89	0.305 ± 0.045	V
306	2015/07/14	4.59	-0.354 ± 0.063	V
313	2015/07/14	6.67	-1.835 ± 0.052	V
313	2015/07/18	5.89	-1.502 ± 0.032	V
324	2015/03/27	11.99	-1.409 ± 0.057	V
337	2015/02/25	18.22	-0.324 ± 0.017	R
426	2015/07/17	17.27	-0.427 ± 0.055	V
426	2015/07/18	17.20	-0.579 ± 0.087	V
444	2015/05/21	6.55	-1.153 ± 0.023	V
444	2015/07/13	15.80	-0.624 ± 0.054	V
444	2015/07/17	17.42	-0.615 ± 0.047	V
478	2015/07/18	7.80	-0.735 ± 0.056	V
478	2015/07/21	8.60	-0.744 ± 0.048	V
478	2015/09/29	17.82	-0.100 ± 0.1	V
491	2015/07/21	11.93	-0.963 ± 0.075	V
500	2015/07/17	7.91	-0.585 ± 0.033	V
511	2015/02/25	9.78	-1.654 ± 0.023	V
532	2015/07/18	21.44	-0.007 ± 0.038	V
679	2015/07/13	3.72	-0.522 ± 0.059	V
690	2015/07/24	21.70	0.559 ± 0.100	V
783	2015/07/21	15.40	-1.319 ± 0.047	V
824	2015/07/13	3.35	-0.735 ± 0.138	V
824	2015/07/15	3.74	-0.904 ± 0.064	V
849	2015/07/17	13.19	-0.713 ± 0.046	V
849	2015/07/18	13.04	-0.755 ± 0.045	V
1372	2015/02/26	19.96	-0.713 ± 0.218	V
1702	2015/05/22	7.39	-1.136 ± 0.550	V